Chemical Science

ROYAL SOCIETY OF CHEMISTRY

EDGE ARTICLE

View Article Online
View Journal | View Issue

Cite this: *Chem. Sci.*, 2023, **14**, 1696

All publication charges for this article have been paid for by the Royal Society of Chemistry

Closing the green gap of photosystem I with synthetic fluorophores for enhanced photocurrent generation in photobiocathodes†

Sascha Morlock, *[ab] Senthil K. Subramanian,[b] Athina Zouni [b] and Fred Lisdat*[a]

Received 23rd September 2022
Accepted 4th January 2023

DOI: 10.1039/d2sc05324a

rsc.li/chemical-science

One restriction for biohybrid photovoltaics is the limited conversion of green light by most natural photoactive components. The present study aims to fill the green gap of photosystem I (PSI) with covalently linked fluorophores, ATTO 590 and ATTO 532. Photobiocathodes are prepared by combining a 20 μm thick 3D indium tin oxide (ITO) structure with these constructs to enhance the photocurrent density compared to setups based on native PSI. To this end, two electron transfer mechanisms, with and without a mediator, are studied to evaluate differences in the behavior of the constructs. Wavelength-dependent measurements confirm the influence of the additional fluorophores on the photocurrent. The performance is significantly increased for all modifications compared to native PSI when cytochrome *c* is present as a redox-mediator. The photocurrent almost doubles from −32.5 to up to −60.9 μA cm^{-2}. For mediator-less photobiocathodes, interestingly, drastic differences appear between the constructs made with various dyes. While the turnover frequency (TOF) is doubled to 10 e^-/PSI/s for PSI-ATTO590 on the 3D ITO compared to the reference specimen, the photocurrents are slightly smaller since the PSI-ATTO590 coverage is low. In contrast, the PSI-ATTO532 construct performs exceptionally well. The TOF increases to 31 e^-/PSI/s, and a photocurrent of −47.0 μA cm^{-2} is obtained. This current is a factor of 6 better than the reference made with native PSI in direct electron transfer mode and sets a new record for mediator-free photobioelectrodes combining 3D electrode structures and light-converting biocomponents.

1. Introduction

Earth's main power source is solar radiation. For over 3 billion years, nature has converted this resource in a process called photosynthesis to produce energy-rich carbohydrates and molecular oxygen as a byproduct.[1–4] In plants and cyanobacteria, this procedure relies on two photoactive protein complexes, photosystems I and II (PSI and PSII). While PSII provides electrons by water-splitting, PSI leads to the reduction of $NADP^+$ in a multi-step process, which is afterward utilized for CO_2 fixation.[2,5–7]

In recent years, many efforts have been made to use this natural potential for the benefit of humanity or, more specifically, for sunlight to electricity conversion.[8–10] In biohybrid photovoltaics, photoactive biocomponents are connected to artificial electrode materials to generate that photocurrent. Successful setups have been achieved with PSI,[1,5,7,11–15] PSII,[9,16–21] and bacterial reaction centers.[4,8,22–25] But likewise, thylakoid membranes[26–28] and even whole cells[29–32] have been deployed effectively.

Many electrode materials and constructions have been applied as the synthetic part in contact with the biological entity. Metals, alloys, and metal oxides such as gold,[8,11,24,33,34] silver,[22] indium bismuth tin,[31] antimony tin oxide (ATO),[25,35] indium tin oxide (ITO),[14,21,28,36–38] titanium dioxide,[16,20,39,40] zinc oxide,[8,29] and zirconium dioxide[39] as well as many carbon-based materials[1,11,21,41,42] have been utilized successfully. It is important to note that not only flat 2D electrodes have been produced,[24,34,43] but also thicker architectures including multilayers,[13,14,24,33] hydrogels,[1,7,23] and 3D setups.[18,20,38,41,44] This is mainly devoted to better light energy usage and reflects the photoactive components' arrangement in a natural thylakoid membrane.

A critical aspect of the overall performance of such biohybrid systems is the interaction of the biocomponent with the electrode material. As a defined orientation of large photosystems is difficult to achieve, often redox-active molecules have been used to shuttle electrons. Examples for these mediators are small redox molecules,[5,18,26,30,32,42] redox polymers[17,19,23,27,28,32,34] or different cytochromes.[12,22,27,35,36,45] The renunciation of redox mediators and,

[a]*Biosystems Technology, Technical University of Applied Sciences Wildau, Hochschulring 1, 15745 Wildau, Germany. E-mail: sascha.morlock@th-wildau.de; flisdat@th-wildau.de*

[b]*Biophysics of Photosynthesis, Humboldt University of Berlin, Philippstraße 13, 10099 Berlin, Germany*

† Electronic supplementary information (ESI) available: Additional information is provided with the spectrum of the light source used in the study, the absorption spectra of two dyes in solution, an SEM image of the 3D ITO electrode structure, photoaction spectra of the different constructs, and data concerning the stability of the photocurrent. See DOI: https://doi.org/10.1039/d2sc05324a

thus, the exploitation of a direct electron transfer provide a less complex system with better-defined electron transfer pathways. However, in general, these approaches result in significantly lower photocurrent densities.[18,32,41,44]

Uncountable steps of evolution have optimized photosynthesis. Once a photosystem captures a photon, it is converted with almost 100% internal quantum efficiency.[2,5,7,14,46] For sunlight absorption, both complexes, PSI and PSII, mainly rely on the green pigment chlorophyll.[1,8,10] Hence, they cannot convert green light efficiently. This limited absorption in the region between 500 and 650 nm is termed the green gap and coincides with the area where the sunlight reaches its peak.[4] Thus, this property of photosystems is one of the main causes for their low external quantum efficiency.[1,2,4,47]

Both nature and science have tried to reduce this limitation. Photosystems do not solely rely on photon absorption by chlorophylls but also contain other pigments. While one primary purpose of carotenoids is the prevention of oxygenic stress, they are also excited by light in the green gap.[48,49] This absorbed energy can be transferred to the chlorophylls, thus increasing the performance of the photosystems.[49,50] Much more efficient, however, are the phycobilisomes in cyanobacteria and red algae. These light-harvesting antenna complexes surround the reaction centers and work well in their absorption gap.[8,51]

In research, photoactive biocomponents have been combined with many different systems that can interact with green light. Here, two different principles can be distinguished. On the one hand, a 2nd photoactive component is integrated into the electrode structure. Here, charge separation occurs in the biocomponent as well as in the 2nd component. Hence, higher cell voltages are obtained and the photoelectrochemical output is improved.[16,20,40] On the other hand, additional light-harvesting dyes have been coupled to photosystems following the natural example to increase the number of excited electrons.

It can be shown that Förster resonance energy transfer (FRET) works for covalently connected synthetic systems, *e.g.*, from Rhodamine Red to the light-harvesting complex,[52] CdTe quantum dots to purple bacterial reaction centers,[53] and Lumogen Red to PSI.[54] Dutta *et al.* have attached three types of Alexa Fluor dyes to genetically modified bacterial reaction centers. Thus they obtained more than twice as much charge separation as in unmodified reaction centers.[55] Gordiichuk *et al.* covalently modified PSI with artificial ATTO 590 dyes and thus improved the electron transfer to oxygen up to 4-fold.[56]

However, despite the many studies demonstrating the upgrading of light-harvesting protein complexes with artificial entities, only a few approaches have been described for applications in photobioelectrodes. Yoneda *et al.* attached fluorophore-modified reaction centers to ITO electrodes and proved a significant photocurrent linked to the absorption maxima of the dyes.[36] This group also demonstrated that the efficiency of excitation energy transfer increases with raising spectral overlap.[57] Yet, overall the photocurrents were very low for both systems.[36,57] Hartmann *et al.* modified PSII with phycobilisomes of three different cyanobacteria and thereby doubled the incident photon-to-current conversion efficiencies in the green gap.[17] Yet, so far, the overall performance of a biohybrid system has not been improved by any modification with synthetic dyes.

The aim of the present study is the first construction of a photobioelectrode based on PSI, which was modified with covalently bound fluorophores. ATTO 590 has been chosen as an artificial dye since the FRET to PSI was proven to be very effective.[56] A three-dimensional structure of ITO nanoparticles has been selected as the synthetic electrode material because of its advantageous properties, particularly a high surface area and good transparency.[15,37,44] Regarding the interaction of the artificial electrode surface with PSI, a mediator based approach exploiting the small redox protein cyt *c* (MET)[37] has been utilized. Additionally, the direct electron exchange of native PSI and the modified PSI constructs with the ITO surface (DET) has also been investigated – based on our recent study.[58] To achieve more than solely a proof-of-principle, this study aims to elucidate the potential of PSI modification for a significant increase in photocurrent density. Thus, another fluorophore (ATTO 532) with a different excitation wavelength has been included in the investigations. Furthermore, PSI constructs with both fluorophores, ATTO 532 and ATTO 590, are evaluated. The study will emphasize that not only conditions of efficient FRET are necessary when modified photoactive complexes are combined with electrodes, but also a productive interaction of the artificial material and the modified biocomponents.

2. Experimental section

2.1 Materials and chemicals

The fluorophores ATTO 590 and ATTO 532, modified as NHS-esters, were bought from ATTO-TEC GmbH, Germany. The chemicals provided by Sigma Aldrich, Germany, were indium tin oxide nanopowder (ITO, <50 nm particle size), latex bead suspension (0.8 μm mean size, 10% in water), methanol (≥99.9%), and *n*-dodecyl-β-D-maltoside (DDM) (>99%), {[1,3-dihydroxy-2-(hydroxymethyl)propan-2-yl]amino} acetic acid (tricine, ≥99%), and cytochrome *c* (horse heart; ≥95%). Roth, Germany, supplied 2-(*N*-morpholino) ethane sulfonic acid (MES, ≥99%), magnesium sulfate (≥99%), 4-(2-hydroxyethyl)-1-piperazineethanesulfonic acid (HEPES, ≥99.5%), potassium dihydrogen phosphate (≥99.5%), orthophosphoric acid (85%), and potassium chloride (≥99.5%). Acetone (ACS grade) and 2-propanol (ACS grade) were purchased from VWR, Germany. Potassium hydrogen phosphate (>99%) was bought from Fluka, Germany, and sodium sulfate (≥99%) from Merck, Germany.

Ultrapure water attained by using a water purifier Aquinity² from Membrane Pure GmbH, Germany, was utilized for the aqueous solutions. For the potassium phosphate buffer (PPB), precalculated amounts of potassium dihydrogen phosphate and potassium hydrogen phosphate were dissolved in water. The pH was then controlled with a pH electrode from Sartorius, Germany. Finally, MES, tricine, and HEPES buffer were prepared by the addition of aqueous KOH to solutions of the respective acid.

2.2 Cultivation, purification, and modification of PSI

The cultivation of *Thermosynechococcus vesticus* and the extraction of the thylakoid membrane proteins were performed as per

Kern *et al.*[59] Using ion-exchange columns, PSI was purified from detergent-solubilized membrane proteins. The PSI trimer received from the second column was crystallized by the 'Salting in' principle using buffer A (5 mM MES-NaOH, pH 6.0, and 0.02% *n*-dodecyl-β-D-maltoside (DDM) at 4 °C, as previously described.[60] The concentration of PSI-bound chlorophyll *a* was determined spectroscopically in buffer A containing 150 mM $MgSO_4$ by $\varepsilon_{680} = 57.1\ mM^{-1}\ cm^{-1}$, and the concentration of the reaction center (P_{700}) was determined by $\varepsilon_{680} = 5.5\ mM^{-1}\ cm^{-1}$.[61] The functional activity of purified PSI was determined by its ability to reduce oxygen upon light illumination, which was measured using a Clark-type electrode, as previously reported.[60]

Immediately before dissolution, the PSI crystals were washed with buffer B (5 mM MES-KOH pH 6, and 0.03% DDM) by centrifuging at 1000 rpm (93 *rcf*) at 4 °C for 5 min. The washing was repeated until the supernatant was colorless and thus free of unbound chlorophyll. Next, buffer C (100 mM tricine pH 9, 150 mM $MgSO_4$, and 0.03% DDM) was added to dissolve the PSI pellet, and the concentration was regulated to 40 μM using UV/vis spectroscopy.

Since comparatively high PSI concentrations are required for the construction of the photobiocathodes, the following procedure was established, inspired by Gordiichuk *et al.*,[56] for the coupling of the fluorophores. 75 μL of the PSI solution was added a tube that was placed in a Thermomixer comfort (Eppendorf, Germany) and cooled down to 4 °C. For the coupling, 31.5 μL of different solutions in dried DMF were added:

- PSI-ATTO590: 20 mM ATTO590.
- PSI-ATTO532: 20 mM ATTO532.
- PSI-ATTO-mix: 20 mM ATTO590 and 20 mM ATTO532.
- PSI-pure: pure DMF (for the reference specimen).

The solutions were kept at 4 °C for 3 h and afterward at room temperature for another 21 h. Then, the solutions were transferred into dialysis cassettes (Slide-A-Lyzer 20 000 MWCO 0.1–0.5 mL capacity) and thoroughly dialyzed *versus* buffer D (50 mM HEPES pH 7, 50 mM $MgSO_4$, and 0.03% DDM) at 4 °C. The dialysate was changed repeatedly until no fluorophore was detected *via* UV/vis spectroscopy. In contrast to previous studies with photobiocathodes, the buffer D was used for the PSI solution to find conditions suitable for all constructs and the unmodified PSI.[37,56,58] Finally, the PSI solutions were set to 20 μM and 4 μM, respectively, and kept at 4 °C.

2.3 Setup of the photobiocathodes

The preparation of the artificial 3D electrode material was conducted as described previously.[58] In brief, a fluorine-doped tin oxide slide (10 × 10 mm) was cleaned by 15 min ultrasonication in each water, 2-propanol, and acetone, and dried at 150 °C for 15 min. Next, it was placed on a KLM Spin-Coater SCC (Schaefer Technologie GmbH, Germany), which was turned to 80 rps. Six drops of the spin-coating mixture (35 mg ITO nanoparticles and 25 mg latex beads in 300 μL methanol : water (6 : 1)) were applied to obtain 20 μm thick ITO structures.

Compared to earlier studies, the protein incubation was slightly modified.[37,58] It was always performed for 3 min in the dark, and excessive biomolecules were removed by rinsing twice with 1 mL buffer as described below. For the test series exploiting MET, 3 μL of 20 μM PSI and 5 μL of 1 mM cytochrome *c* (cyt *c*, in buffer E (5 mM PPB pH 7)) solutions were utilized and buffer E was applied for rinsing and the execution of the electrochemical measurements. Electrodes relying on DET were incubated with 4 μL 4 μM PSI solution. They were then rinsed and measured using buffer F (100 mM MES pH 6 and 400 mM KCl). Controls without PSI were conducted, too. Here, the pure ATTO dyes were dissolved in buffer D. 7 μL of the solutions were applied for 3 min in the dark. Equivalent fluorophore concentrations were present as in the incubation for the DET-based photobioelectrodes. This means 48 μM ATTO 532, 44 μM ATTO 590 or 44 μM ATTO 532 & 32 μM ATTO 590 (ATTO-mix), respectively. Then, the electrodes were rinsed and measured with buffer F.

2.4 (Photo-)electrochemical experiments

A three-electrode arrangement was utilized for all electrochemical measurements, in which the photobiocathode acted as the working electrode. The counter electrode was a platinum wire along with an Ag/AgCl/3 M KCl reference electrode (DRIREF-2SH from World Precision Instruments, USA). The photoelectrochemical experiments were conducted at the workstation Zennium PP210 by Zahner, Germany. Usually, a white light source was used at an intensity of 100 mW cm^{-1} unless stated otherwise (for the spectrum, see Fig. S1†). For the measurements of the photocurrent, *i.e.* the change in the current flow between dark and illuminated states, an overpotential of −100 mV *vs.* Ag/AgCl was applied. The turnover frequency was determined as the ratio of the photocurrent divided by the number of PSI trimers.

During chopped-light voltammetry, 5 s light pulses were applied repeatedly while the potential was varied at 2.5 mV s^{-1} from 463 to −300 mV *vs.* Ag/AgCl. Photo-action spectra were obtained by illuminating the photobioelectrode with the light of different wavelengths generated by a Polychrome V (FEI, USA) and recording the photocurrent response at −100 mV *vs.* Ag/AgCl.

2.5 Calculation of the loading with biomolecules

The PSI and PSI-construct coverage on the 3D electrodes was determined similarly to before.[58] The electrodes were prepared with 8 × 8 mm dimensions to fit into a test tube. Only the edges of the slides were cleaned from excessive ITO material to allow for a defined, large area. For mediator-free electrodes, the preparation followed the procedure under Section 2.3. Yet, 7 μL of 4 μM PSI solution were used for incubation to allow for a greater area. After the preparation, the biohybrid structures were kept in buffer F for 25 min. The following day, the structures were placed into 500 μL 80% acetone for 60 min for chlorophyll extraction. The UV/vis absorption at 664 nm was used to calculate the PSI concentration. The electrodes containing cyt *c* were handled analogously. However, 5 μL of 20 μM PSI and 10 μL of 1 mM cyt *c* solutions were used and buffer E was applied instead.

To determine the cyt *c* loading, cyclic voltammetry (CV) was utilized, similar to reported.[37] For this purpose, scans of the

photobioelectrodes were recorded in the dark at a rate of 10 mV s^{-1} from −200 to +300 mV *vs.* Ag/AgCl. The area below the peak (faradaic current) correlates with the number of transferred electrons and, thus, with the number of adsorbed cyt *c* molecules.

2.6 Further measurements

An Evolution 300 UV/vis spectrometer (Thermo Scientific, Germany) was used in the range from 350 to 750 nm at a rate of 600 nm min^{-1} for the absorbance measurements. Scanning electron microscopy (SEM) was executed with a JSM-6510 (JEOL, Japan). Fluorescence was studied after excitation at the absorbance maxima of the dyes, 532 and 590 nm, respectively. A Cary Eclipse Fluorescence Spectrometer (Varian, USA) was utilized.

The O_2 consumption of the constructs was measured in solution in buffer G (5 μM chlorophyll in 5 mM tris pH 7, 16 μM cyt *c*, 0.2 mg mL^{-1} sodium ascorbate, 0.05 mg mL^{-1} methyl viologen, and 0.02% DDM) with a Clark-type electrode (Oxygraph$^+$, Hansatech, Germany) as reported previously by application of cyt *c* as an electron donor to the luminal side of PSI.[60]

3. Results and discussion

3.1 Characterization of the PSI-ATTO-constructs

The present work aims to increase the photocurrent density of photobioelectrodes by modifying PSI with synthetic fluorophores. Here, two dyes (ATTO 590 and ATTO 532) have been selected with two different absorption maxima in the green gap (*ca.* 590 nm and 532 nm respectively; for absorbance spectra see Fig. S2†). These molecules have been covalently coupled to PSI *via* NHS chemistry (see Section 2.2). Additionally, to the single fluorophore coupling to PSI, both fluorophores have also been bound. The latter construct is termed, here, PSI-ATTO-mix. As a first step, the constructs have been examined to verify the successful coupling. To this end, UV/vis spectroscopy has been conducted in buffer D solution. All three constructs have been purified by dialysis after the coupling reaction. In the solution, there is no unbound fluorophore present since no fluorophore could be detected in the dialysate during purification. Therefore, the signals at 590 and 532 nm, respectively, can be attributed to covalently attached dyes. Fig. 1A shows clearly that the coupling has been successful. Distinct peaks are visible in the green gap, where PSI does not absorb well as shown by the reference spectrum. The spectra can also be used to quantify the coupling efficiency. A summary of the obtained coupling ratios is given in Table 1. For comparison, only data of the coupling of ATTO 590 can be found in the literature, and the results are similar.[56] Slight differences occur since for the present investigations high PSI concentrations are necessary for the subsequent immobilization in the 3D electrode structure. Thus, for all coupling experiments, a PSI concentration of 28 μM (compared to *ca.* 1 μM in the literature) has been used.

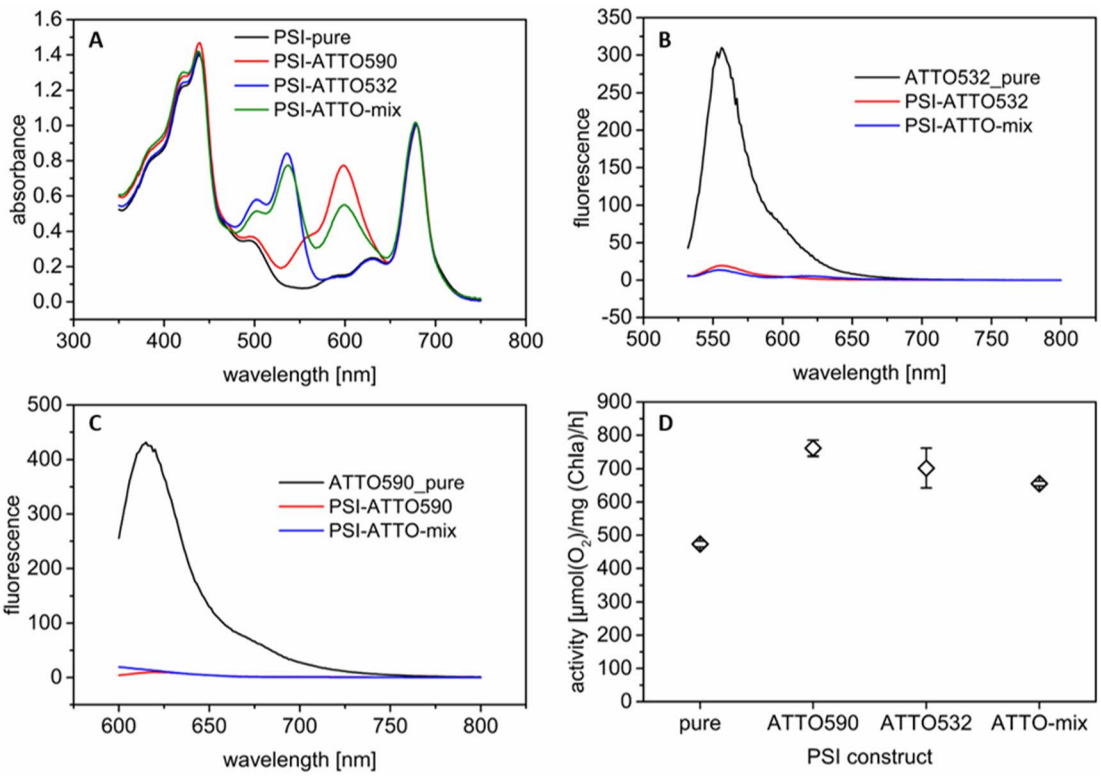

Fig. 1 (A) to (C) Spectra of the constructs and pure ATTO dyes in buffer D. (A) Absorbance of the PSI-ATTO variants normalized at 680 nm; (B) fluorescence spectra after excitation at 532 nm (ATTO532_pure: ATTO dye in absence of PSI); (C) fluorescence after excitation at 590 nm (ATTO590_pure: ATTO dye in absence of PSI); (D) comparison of the oxygen consumption of the different PSI constructs in solution with cyt *c* as the electron donor (see Section 2.6). Pure: unmodified PSI ($n = 3$); ATTO590: PSI-ATTO590 ($n = 3$); ATTO532: PSI-ATTO532 ($n = 4$); ATTO-mix: PSI-ATTO-mix ($n = 3$).

Table 1 Degree of labeling (DoL) for the 3 modified PSI used in this study. The values were determined by UV/vis spectroscopy in buffer D and are stated as dyes per PSI trimer (n.a. – not applicable)

Construct	DoL (ATTO 590)	DoL (ATTO 532)
PSI-ATTO590	11	n.a.
PSI-ATTO532	n.a.	12
PSI-ATTO-mix	8	11

To evaluate the FRET within the constructs, fluorescence measurements have been executed. Fig. 1B and C show that the fluorescence of all the tested chromophores is drastically quenched when they are connected to PSI compared to pure ATTO molecules in solution. This indicates that FRET is feasible for the three constructs. For the PSI-ATTO532 variant, a small fluorescence peak remains while it is not present for PSI-ATTO590. The latter is in line with the literature.[56] This implies that FRET in the PSI-ATTO590 construct is slightly more effective due to the higher overlap of the fluorescence emission with the absorption of PSI. Yet, for the PSI-ATTO532 construct also a significant energy transfer is achieved as the fluorescence peak's height is reduced by one order of magnitude. In the PSI-ATTO-mix construct, only a small fluorescence signal remains after excitation. This indicates that here energy transfer is slightly more efficient than with only ATTO532 coupling to PSI. The FRET can also be verified by evaluating the PSI fluorescence with excitation at 532 nm or 590 nm (see Fig. S3†). Here the fluorescence intensity is increased after coupling the dyes to the photoactive complex.

Furthermore, the activity of the different constructs has been assessed. Thereto, the O_2 consumption has been determined under illumination with cyt *c* as the electron donor. The results shown in Fig. 1D illustrate that all variants are very active. The modified PSI constructs perform significantly better since they can absorb more photons from green light due to the attached dyes. The O_2 consumption is approximately doubled for all modifications. There is no clear trend visible. As indicated in the fluorescence measurements, the performance of the PSI-ATTO532 variant is also boosted despite the lower spectral overlap.

After demonstrating successful coupling and functional energy transfer for all three PSI constructs, they have been subsequently studied as a photoactive component in photobiocathodes.

3.2 Working principle

The properties of the photoactive protein complex have been altered by attaching the dyes to the trimeric PSI from *Thermosynechococcus vesticus* as indicated in Fig. 2. Such coupling affects not only the absorption spectrum, but also other properties. For example, the modified PSI is no longer soluble in 5 mM MES pH 6 with added 60 mM $MgSO_4$ and 0.02% DDM, although this buffer works well for native PSI.[60] Hence, its behavior in photobioelectrodes might also be impacted and will, thus, be investigated here.

For the study, 3D ITO electrodes have been used, which can be prepared easily by a template-based approach combining spin-coating depositions with a heating step for template removal and ITO sintering. This procedure allows tuning the thickness in the range of 10 to 30 μm providing thus an attractive 3D space for PSI immobilization.[58] The open 3D structures have been verified by SEM investigations as given in Fig. S4.†

Two strategies have been tested to connect PSI and the three PSI constructs with the electrode: (i) a mediator-based approach applying cyt *c* and (ii) a mediator-free setup with direct electron exchange between ITO and PSI. The former has already been observed several times in the literature.[15,37,38] For the latter, it has been shown recently by ourselves that conditions can be found to increase the performance significantly.[58]

For the immobilization of the native protein and the constructs, direct assembly on 3D ITO has been exploited which is fast and efficient. The same is valid for cyt *c* deposition. This redox active protein was co-immobilized with PSI in some of the photobiocathodes to shuttle the electrons to PSI. The mediation of electron transfer between PSI and electrodes by means of the small redox protein has been previously carefully analyzed and is thus not in the focus of the present study.[34,37,60] The following conditions have been applied for all constructs – 4 μM PSI solutions for electrode preparation in DET mode and 20 μM PSI and 1 mM cyt *c* solutions for MET for 3 min each. However, the different surface properties of the different PSI variants may influence the adsorption efficiency within the short time interval of immobilization, as studied in Section 3.6. In all the experiments, no additional electron acceptor has been added to the solution so that the oxygen in the air-saturated buffer is the final electron acceptor.[35,62] In the case of cyt *c* containing electrodes (MET), the electrons are transferred from the electrode towards this redox protein first and then to the excited PSI. The electrons are transported along the in-built electron transfer chain towards the stromal side where they can be passed to molecular oxygen. For cathodes without cyt *c* and, thus, without any mediator present in the setup, the electrons are transferred directly from the ITO material to the luminal side of the PSI complex (DET). Then the electrons follow the same pathway as described for the MET system.

Different photoelectrochemical techniques have been applied to characterize the electrodes with PSI and the three PSI constructs, as will be explained in the following three subsections. They confirm the behavior of PSI-ITO hybrid structures as photobiocathodes. Finally, it must be noted that for ITO/PSI/cyt *c* electrodes, a buffer E (5 mM PPB pH 7) is used during operation, whereas for the ITO/PSI electrodes in DET mode, buffer F (100 mM MES buffer pH 6, and 400 mM KCl) is applied. These conditions provide a suitable setting for the respective setups.[37,58]

3.3 Potential behavior of the photocurrent

The first series of tests have been performed with chopped-light voltammetry on electrodes with the different constructs. Therefore, the applied potential has been varied in a wide range while white light at 100 mW cm^{-2} has been turned on and off repeatedly. The results of such experiments are compiled in Fig. 3. At first glance, it is evident that the setup of photobioelectrodes is successful for all constructs for both MET and DET as envisioned

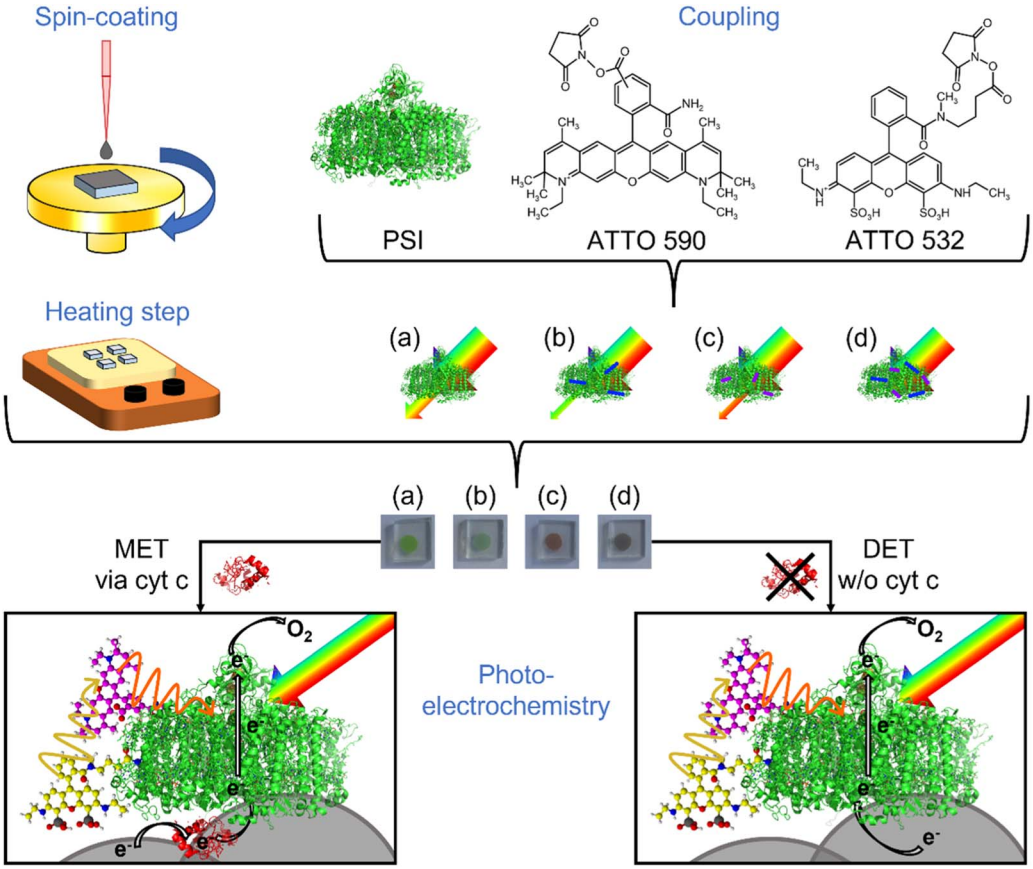

Fig. 2 Working principle of the photobiocathode. Top left: Sketch of the preparation of the artificial 3D ITO structure by spin-coating and a baking step. Top right: Coupling PSI and the 2 ATTO dyes and illustration of their different UV/vis absorbance properties. Symbolization of the constructs: PSI-pure (a), PSI-ATTO590 (b), PSI-ATTO532 (c), and PSI-ATTO-mix (d). Center: Photographs of biohybrid setups prepared by immobilization of the constructs onto 3D ITO (labeling (a) to (d) as before). Bottom: Electron pathways for the two evaluated electron transfer mechanisms. When light hits the electrode, only non-green light can be converted by PSI. ATTO 590 and ATTO 532 are excited by light in this green gap. Curved arrows indicate the direction of the energy flow *via* FRET. Two principles are exploited to refill the electron into P700, MET *via* cyt *c* (left) or DET without a mediator and direct interaction of the ITO with the luminal side of the protein complex (right).

in Section 3.2. While only slight signs of anodic currents have been obtained at higher applied potentials, clear photocathodic responses can be verified.

The experiments also enable the determination of the onset potential of the cathodic photocurrent. The electrodes based on mediation depend on the redox potential of the applied cyt *c*. Here, cathodic photocurrents start at about +100 mV *vs.* Ag/AgCl for all constructs. This finding is in line with the literature.[37] By decreasing the potential, the photocurrent can be further enhanced, but potentials lower than −100 mV *vs.* Ag/AgCl do not increase the current output substantially.

For DET, the first cathodic photocurrents are obtained at higher potentials. Interestingly, here, significant differences appear for the constructs. The highest onset potential can be found for the unmodified PSI. At 400 mV *vs.* Ag/AgCl, it corresponds well to the values seen before.[58] The cathodic photocurrents for the constructs start at slightly lower potentials ranging from 250 to 325 mV *vs.* Ag/AgCl. Also, for the electrodes operating in DET mode, a lower potential has been found beneficial for a further gain in photocurrent. From these evaluations, the working potential for the photocurrent measurements can be determined as well. For all experiments, an applied potential of −100 mV *vs.* Ag/AgCl is chosen since high currents can be achieved, here, at relatively low overpotentials. Additionally, this potential enables good comparability to previous studies.[37,58]

3.4 Verification of the dyes in the photocurrent measurement

Photo-action spectroscopy has been executed next, to prove that the presence of the fluorophores leads to a better performance of the constructs in the green gap. Therefore, the photobiocathodes have been illuminated with light of different wavelengths. The results of these experiments are compiled in Fig. 4 and S5.† For the PSI-ATTO590 construct, FRET has been reported before,[56] but here it can be demonstrated that this can be exploited beneficially for the current generation in photobiocathodes. Interestingly, also for the PSI-ATTO532 variant, an additional photocurrent

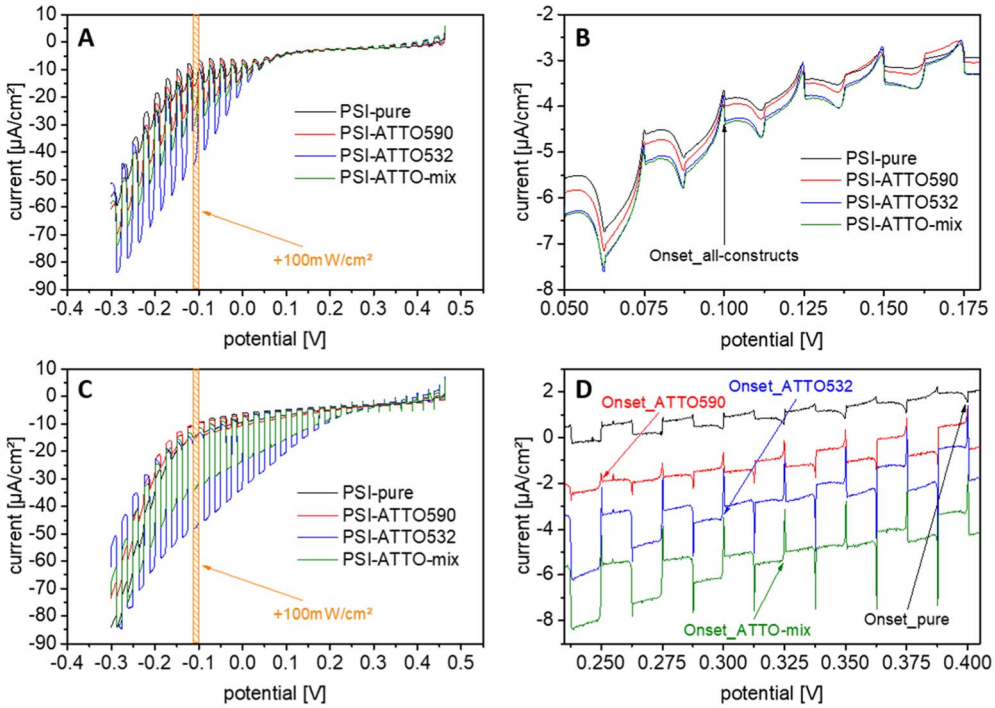

Fig. 3 Chopped-light voltammetry and determination of the onset potential of the cathodic photocurrent and the optimal working potential for the photobioelectrodes based on (A and B) MET and (C and D) DET. Yellow bars in A & C are exemplary for one 5s-window, where the light is turned on. For better visibility some curves are shifted in D with +4 µA cm^{-2} (PSI-pure), +2 µA cm^{-2} (PSI-ATTO590), and −2 µA cm^{-2} (PSI-ATTO-mix).

compared to electrodes with native PSI alone can be obtained at around 540 nm.

When both dyes are coupled to PSI (PSI-ATTO-mix), it can generate photocurrents in the wavelength range of both fluorophores. Such photocurrent can be seen for electrodes with cyt *c* (MET) as well as electrodes based on DET.

In conclusion, one can state that the presence of the fluorophores can be verified on a functional level. It results in an improved photocurrent generation in the green gap compared to unmodified PSI. This finding corresponds well to concepts in the literature.[17,36,39,57]

3.5 Photocurrent response

As stated previously, the main goal of the application of the fluorophore-modified constructs instead of native PSI is the improvement of the performance of the photobiocathodes. Hence, after the proof of principle that the dyes can be seen in the green gap during photo-action spectroscopy (Section 3.5), photocurrents have been measured. Like before, 3D ITO electrodes of about 20 µm thickness and a white light source at 100 mW cm^{-2} have been used for all experiments. A constant potential of −100 mV *vs.* Ag/AgCl is applied as discussed in Section 3.3.

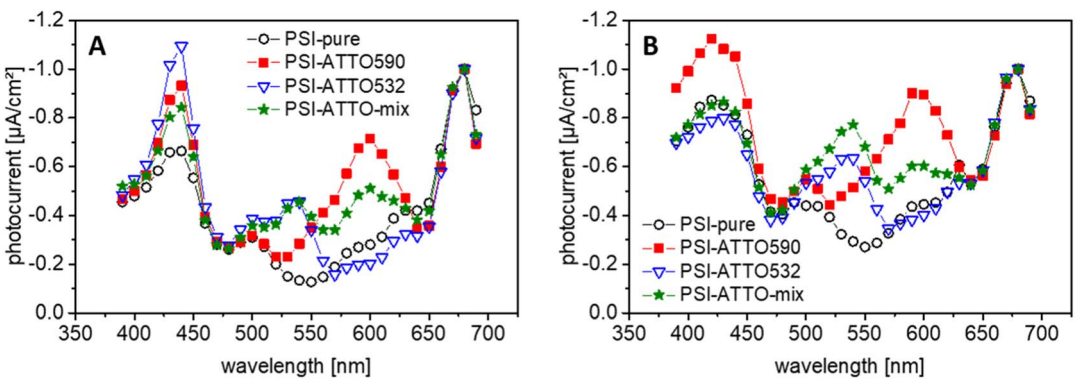

Fig. 4 Photo-action spectra of the photobiocathodes based on the different constructs. (A) MET with cyt *c* and the constructs on 3D ITO in 5 mM PPB pH 7; (B) DET without a mediator in 100 mM MES pH 6 and 400 mM KCl.

3.5.1 Photobiocathodes based on cyt *c* as the mediator. The photocurrent densities for PSI and the three constructs are depicted in Fig. 5A. For unmodified PSI, photocurrents of -32.5 ± 3.6 μA cm^{-2} have been obtained for electrodes based on MET. These numbers correspond well to the literature for such a system.[37]

The performance of all constructs differs significantly from that of the non-modified reference. The PSI-ATTO590 construct works drastically better than the PSI alone (-55.3 ± 7.0 μA cm^{-2}). The PSI-ATTO532 variant performs slightly better but is still within the error bars of both values (-60.9 ± 9.5 μA cm^{-2}). The PSI-ATTO-mix construct also shows a significant photocurrent increase (-50.1 ± 6.4 μA cm^{-2}) compared to electrodes with native PSI, but no further enhancement is achieved compared to the constructs with only one fluorophore. These findings show a comparatively large enhancement when the absorption spectra of PSI and the constructs are considered only, but they match well with the activities of natural and modified PSI (measured by oxygen consumption in solution – see Section 3.1), which has been found enhanced for all three constructs by a factor of about 2. This means that the enhanced activity found in solution (which includes not only the light interaction but also the cyt *c* reaction) is well reflected in the electrode performance of the constructs with respect to the non-modified PSI.

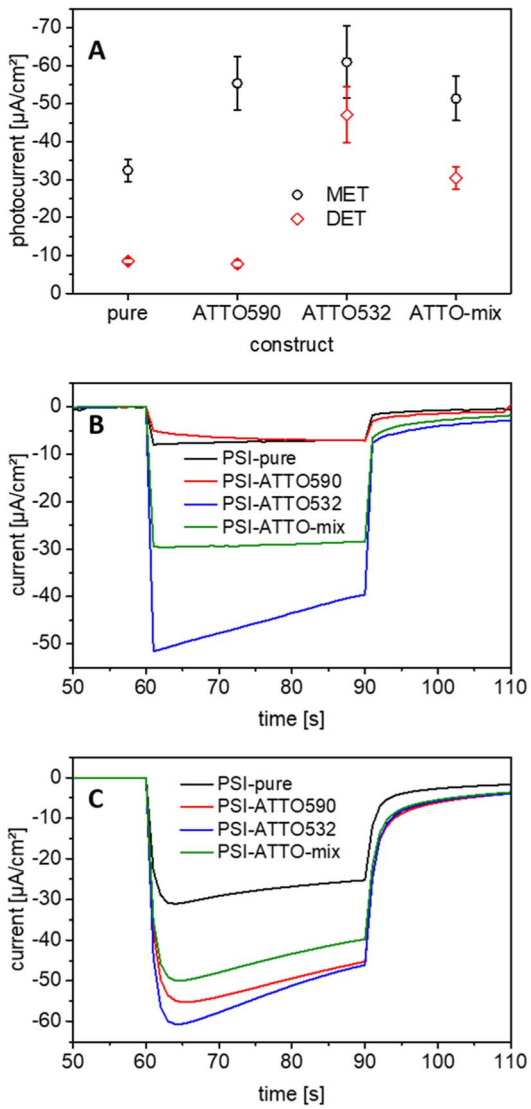

Fig. 5 Performance of the biohybrid setups prepared by the different constructs. Pure: PSI-pure; ATTO590: PSI-ATTO590; ATTO532: PSI-ATTO532; ATTO-mix: PSI-ATTO-mix. (A) Photocurrent of the photobiocathodes relying on MET and DET. Pure: MET ($n = 4$) and DET ($n = 7$); ATTO590: MET ($n = 4$) and DET ($n = 4$); ATTO532: MET ($n = 4$) and DET ($n = 11$); ATTO-mix: MET ($n = 4$) and DET ($n = 3$); (B and C) representative photocurrent measurements for (B) DET and (C) MET respectively. Photocurrent measurements conducted in buffer F for DET and buffer E for MET at -0.1 V *vs.* Ag/AgCl and 100 mW cm^{-2} illumination.

3.5.2 Photobiocathodes based on DET from the ITO electrode. The evaluation of DET-based electrodes and, thus, systems avoiding an additional component exhibits more remarkable differences in the performance caused by the various constructs. Photobiocathodes based on native PSI achieve photocurrents of -8.5 ± 0.8 μA cm^{-2}, which matches well with the literature.[58] Interestingly, electrodes with the PSI-ATTO590 construct do not provide a higher photocurrent compared to this unmodified reference (-7.7 ± 1.0 μA cm^{-2}). Furthermore, their current response kinetics is much slower than for PSI and the other variants, as illustrated in Fig. 5B. In contrast, the PSI-ATTO532 variant shows some extraordinary effects within the 3D ITO electrode structure: the photocurrents are almost 6-fold higher for this construct (-47.0 ± 7.4 μA cm^{-2}) compared to unmodified PSI. This increase surpasses the increment observed in the UV/vis study as well as in the activity measurements (Section 3.1) and, thus, cannot be explained by the additional absorption of light in the green gap alone. An important hint can be obtained when the non-normalized photo-action spectra are compared (Fig. S6†). Here, the photocurrent enhancement occurs in the whole wavelength range studied. This means that even for wavelengths, which are not absorbed by the fluorophore, the photocurrent is significantly higher than for the other electrodes. Photobiocathodes using PSI-ATTO-mix exhibit an intermittent behavior compared to PSI-ATTO590 and PSI-ATTO532 electrodes (-30.4 ± 3.0 μA cm^{-2}).

Previously, it was already verified that without PSI no significant photocurrents can be obtained on bare nanoparticular 3D ITO electrodes.[58] To rule out that the dyes interacting with the artificial surface define the photocurrent output, control measurements with the dyes only have been conducted. The obtained current responses are depicted in Fig. S7.† No clear photocurrent signals can be determined. This demonstrates that PSI is the photoactive component responsible for photocurrent generation, which is influenced by the coupled dyes as illustrated in Fig. 2.

3.5.3 Comparison of MET and DET modes. While the photocurrent density is in general significantly higher for MET, also other differences appear between the two electron transfer mechanisms. As just discussed, the kinetics for the DET to PSI-ATTO590 is poor, whereas the current response is very fast for the other systems. Here, when no mediator is present, the maximal photocurrent is reached within the first second after switching-on the light. In contrast, for MET the kinetics is

slower but similar for all variants. It takes about 5 s to reach the maximum current density as depicted in Fig. 5C.

As shown, the covalent binding of fluorophores to PSI changes its optical properties but has also other effects that are essential when applying such constructs in photobioelectrodes. Two main reasons can be seen for the different photocurrent output of electrodes in both MET and DET modes: the coupling of dyes to the PSI surface can impact the number of immobilized protein complexes and their orientation to the ITO surface. While the first aspect directly influences MET- and DET-based electrodes, the latter is of higher relevance for electrodes in DET mode. Thus, the number of immobilized biomolecules has been studied and will be discussed in the next section with respect to the photocurrent behavior illustrated above.

3.6 Protein coverage on the photobioelectrodes

The coverage with biomolecules has been determined to trace possible causes for the performance differences of the constructs. For this purpose, chlorophyll has been extracted from the electrodes after preparation like described in Section 2.5. As can be seen in Fig. 6A, significant differences appear. It must be noted that the electrode preparation has not been identical for photobiocathodes operating in MET and DET modes (see Section 2.3).

For MET, after the incubation with PSI, cyt *c* is applied. This additional incubation in a highly concentrated cyt *c* solution can disrupt the binding of PSI to the ITO surface. Here, the unmodified PSI shows the highest adsorption to the ITO surface, whereas the PSI constructs result in somewhat smaller surface concentrations. When the cyt *c* coverage is analyzed, similar electro-active concentrations have been found, with a small peak for electrodes with the PSI-ATTO532 variant.

Since the number of bound PSI constructs is diminished for electrodes operating in MET mode (compared to the native protein complex), but the photocurrents are found to be larger, a significantly higher turnover number can be elucidated for the electrodes with the fluorophore-coupled PSI. The highest values are obtained here for the PSI-ATTO532 and the PSI-ATTO-mix construct (105 e^-/PSI/s). However, in the latter case the amount of immobilized photoactive protein is the smallest; consequently, the overall photocurrent enhancement is the lowest among the constructs (although significant).

Evaluating the electrodes prepared in DET mode, again the highest surface concentrations have been found for the native protein complex (18.4 ± 1.0 pmol cm^{-2}). Slightly smaller values are obtained for PSI-ATTO532 and PSI-ATTO-mix, 15.8 ± 1.3 pmol cm^{-2} and 14.7 ± 0.8 pmol cm^{-2}, respectively. The PSI-ATTO590 loading falls out of line. Here, just 7.8 ± 0.4 pmol cm^{-2} is bound to the ITO electrode material which is a factor of 2 lower than that for the other constructs.

This low coverage can explain the poor performance of the PSI-ATTO590 construct on the 3D ITO in DET mode. When the turnover frequencies (TOFs) are compared (Fig. 6B), it stands out that this variant performs about 2 times better than the reference specimen, 10 *vs.* 5 e^-/PSI/s. This is in line with the oxygen consumption activity (Section 3.1), where the same difference in the turnover rate appears. The highest TOF is obtained for the PSI-ATTO532 modification with 31 e^-/PSI/s, which is a factor of 6.5 better than that of the natural PSI. The value for PSI-ATTO-mix lies between the others at 21 e^-/PSI/s.

The disparity between the constructs might be explained by the chemical structure of the dyes. Although they are rather similar, there are some differences that are necessary to obtain different optical properties. ATTO 590 consists of 5 condensed aromatic rings; thus, it is hydrophobic. In ATTO 532, two sulfo groups provide a higher hydrophilicity and a negative net charge. These differences could lead to some consequences: both dyes bind in different areas of the PSI molecules and/or they change the binding behavior of the modified PSI to the ITO structure, *i.e.*, the number and orientation, of the adsorbed constructs. The former is a probable explanation for the PSI-ATTO590 electrode behavior since here less construct binds to the ITO structure. In contrast, PSI-ATTO532 performs better than envisioned although the PSI loading is not enhanced compared to the unmodified protein complex. Hence, the most likely reason for the better output is that the ATTO 532 dyes aid in an accurate orientation of PSI towards the ITO nanoparticular surface. This conclusion originates from the fact that

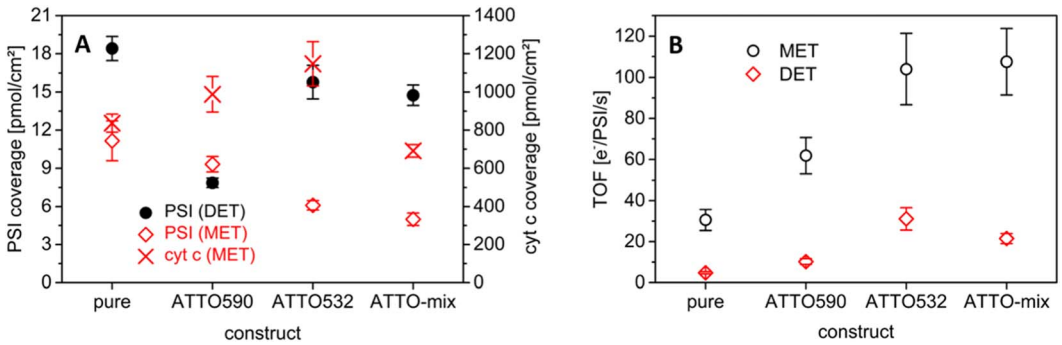

Fig. 6 Comparison of the biocomponents in the photobiocathodes. (A) PSI and cyt *c* coverage of the structures; for electrodes in DET mode the only present biomolecule is PSI (black dots), and in the case of MET-based electrodes, two numbers – for PSI (red squares) and cyt *c* (red crosses) – are given; $n = 4$ for PSI (DET) ATTO590 and ATTO-mix, and $n = 3$ for the remaining; (B) turnover frequencies of the diverse electrodes calculated by using the values of Fig. 5A and 6A

a rather similar amount of the photo-active protein is immobilized in the 3D ITO for the native PSI and the PSI-ATTO532 construct, but a significantly higher photocurrent is observed for the modified protein. This means that a larger fraction of the photoactive complexes is in a productive orientation with respect to the ITO surface for the construct-based electrode. This explanation is strongly supported by the finding that the photocurrent with the ATTO532 construct is enhanced in the whole wavelength range used in photo-action spectroscopy, *i.e.*, even at wavelengths where this dye does not absorb light (Fig. S6†). In summary, one can state that the fluorophore modification helps not only in photon collection, but also in optimizing the interaction of the photoactive protein complex with the electrode surface. The intermittent behavior of PSI-ATTO-mix seems to be consistent with the discussed effects for attached ATTO 532 and ATTO 590 for the interaction with the ITO structure. Further studies will, however, be necessary to elucidate the details of the fluorophore coupling to PSI and the interaction of the resulting constructs with the ITO surface.

3.7 Evaluation of the PSI-ATTO532 photobiocathode

Since the PSI-ATTO532 construct outperforms the other variations in DET mode on 3D ITO and the expectations from the additional light interaction in the green gap, further measurements have been conducted to accumulate more information about this photobiocathode. First, the photocurrent response at different illumination intensities has been evaluated. So far, all experiments have been executed at 100 mW cm^{-2}, which roughly corresponds to the power of solar radiation. Now, the illumination intensity has been reduced stepwise by 3 orders of magnitude down to 0.1 mW cm^{-2}. The results are depicted in Fig. 7A. An almost linear increase of the current response with the light intensity is obtained even for high intensities, which is remarkable.

Another critical aspect of photobioelectrodes is their stability under repeated illumination. Thus, 30 light pulses with a duration of 2 min each have been applied onto PSI-ATTO532 photobioelectrodes. The photocurrent response is relatively stable, but tends to decrease over time, as illustrated in Fig. 7B and S8.† After two hours of light treatment, a total of 60 min illumination, the initial performance is halved. This is significantly better than findings in many previous studies when usually 50% of the starting value is reached after $1/4^{th}$ of this time period.[38,41,63] However it has to be noted that the reported photobioelectrodes have been relying on MET.

Better stability has been found for DET-based electrodes with unmodified PSI.[58] However, in the present study, much higher photocurrents have been obtained with the fluorophore-modified PSI so that even after more prolonged operation, much higher photocurrent values can be retained compared to the unmodified PSI.

3.8 Classification of the findings

As stated in the Introduction, only a few studies have been undertaken with modified biomolecules to close the green gap in photobioelectrodes. Light-harvesting bacterial reaction center core complexes were modified with four different dyes (Alexa 647, Alexa 680, Alexa 750, and ATTO 647N) and coupled to ITO electrodes. By that, 1.6 and 1.8 μA cm^{-2} were achieved,[36,57] which is 35 times less than that obtained in this study.

Takekuma *et al.* combined TiO_2, PSI, and a perylene di-imide derivative to measure photocurrents up to 430 μA cm^{-2}.[39] Yet, it must be noted that most photocurrent is already available without the photosystem. Since the electrolyte contained guanidine thiocyanate, it is also questionable whether the proteins were still intact during measurement. Additionally, no photo-action spectra or similar experiments are shown to verify PSI as the current source.

Some photobioelectrodes applying non-modified PSI have been reported in the literature and can be used for comparison with these novel photobiocathodes to some extent. However, most of the studies have been using a mediator to improve the performance. As stated in Section 3.5, the values obtained for the reference specimen (native PSI) compare well to earlier results with the same electrodes.[37]

Hence, the photocurrent output, up to -60.9 ± 9.5 μA cm^{-2}, of the fluorophore-modified electrodes is 2-times higher than that for natural PSI-based ones under similar conditions (here,

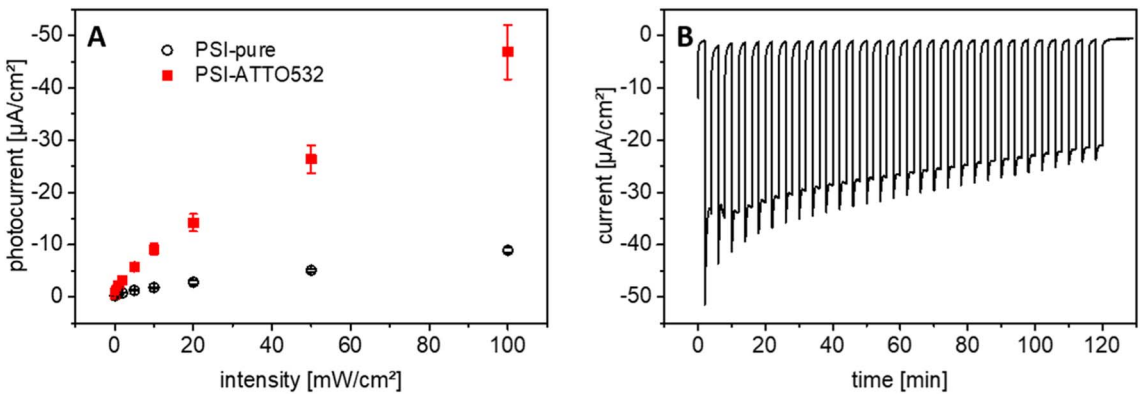

Fig. 7 Photocurrent measurements of photobiocathodes without a mediator in 100 mM MES pH 6 and 400 mM KCl at an applied potential of −100 mV *vs.* Ag/AgCl. (A) Comparison of the performance of PSI-ATTO532 ($n = 4$) and native PSI ($n = 3$) at different light intensities; (B) behavior over two hours of 3 electrodes (mean value) prepared with PSI-ATTO532.

MET mode with cyt *c* as the immobilized mediator). This clearly demonstrates the potential of improving the spectral properties of PSI for enhanced light-to-current conversions.

The measurements demonstrate that besides the optical properties, the binding to the surface can be impacted by the fluorophore coupling. This can also compensate for improved light interactions, as shown for electrodes with PSI-ATTO590 and cyt *c* as mediator.

There is also a significant development in new electrode materials. For example, a more transparent ITO electrode can be prepared when starting from solutions of precursor compounds instead of nanoparticles as done in this study. Such electrodes have already resulted in much higher photocurrents.[38] Thus, this will open more opportunities for using fluorophore-coupled PSI to increase photocurrent output further.

In the literature, not many values obtained by DET are available for comparison. However, in a previous study, 10.1 μA cm^{-2} was achieved for a similar electrode after an intensive evaluation of the measurement conditions.[58] This benchmark is outperformed by a factor of 5 by PSI-ATTO532 with even thinner ITO electrode structures. Here it can be stated that besides the filling of the green gap of PSI, mainly a better interaction of the luminal side with the ITO surface contributes to the substantial performance increase while retaining the adsorption capability of the PSI construct to the 3D ITO material. To the best of our knowledge, 47.0 μA cm^{-2} is the record value for DET of any photoactive biomolecule on a 3D material. The previous record – 33 μA cm^{-2} set for PSII on 3D ITO is surpassed by a factor of *ca.* 1.5.[64]

An interesting aspect is the comparison of the performances of electrodes based on the two evaluated electron transfer mechanisms. When similar photobioelectrodes have been tested before, DET has often been found to be far more than one order of magnitude less effective than MET.[9,21,37,38,41] Although the direct interaction between ITO and PSI has been thoroughly studied recently and parameters have been optimized,[58] this pathway is still about a factor of 4 less effective for natural PSI as shown in the present study (−8.5 compared to −32.5 μA cm^{-2} in MET). However, owing to coupled ATTO 532, this gap narrows drastically so that the mediator-less system achieves more than 3/4 of photocurrent density of the setup with incorporated cyt *c* (−47.0 *vs.* −60.9 μA cm^{-2}). Furthermore, these new photobiocathodes based on DET and PSI-ATTO532 outperform the established mediator-based electrodes with natural PSI and cyt *c* by about 50% (−47.0 *vs.* −32.5 μA cm^{-2}).

4. Conclusions

In the study at hand, photobiocathodes based on 3D ITO are described, which exploit fluorophore-modified PSI to close its green gap. The dyes can be proven to provide an additional signal at their absorbance maxima in wavelength-dependent measurements and contribute significantly to the constructs' performance.

In one approach of electrode construction, cyt *c* has been applied as a mediator to shuttle electrons to PSI. Here, all modified photosystems outperform the natural one up to a factor of about two. The TOF has also been increased for all constructs; up to 105 e^-/PSI/s have been measured for photosystems that have been altered with both dyes, ATTO 590 and ATTO 532.

Significant differences are obtained for the mediator-less approach (DET mode). Since PSI-ATTO590 weakly binds to the ITO structure, its photocurrent is lower than that of the reference specimens, although the TOF is doubled. In contrast, PSI-ATTO532 binds nearly as effectively as native PSI to the 3D ITO and the dye most likely aids in the orientation of the construct towards the surface. Thus, the photocurrent density and TOF increased tremendously to −47.0 μA cm^{-2} and 31 e^-/PSI/s, respectively.

The findings presented, here, offer many new opportunities, especially for mediator-less approaches, since major differences have been obtained depending on the modification. Another interesting prospect of biohybrid photovoltaics is the coupling of the photoactive setup to enzymes for the conversion of specific molecules. Therefore, high photocurrents are desirable because they provide more electrons. However, efficient communication between all components is essential as well. By now, it remains open whether this interaction is impeded or aided by the presence of the fluorophores.

Due to this study, the stimulating question emerges what other modifications might be advantageous for PSI or other biocomponents in general for the interaction with artificial materials. In the present work, only minor changes have been made (by coupling 11 to 19 fluorophores to the large trimeric PSI complex), leading to massive behavioral alterations. The performance of PSI-ATTO532 on 3D ITO in DET mode is boosted for all wavelengths; hence, this aspect is not limited to light-converting components. Since the interaction is generally improved, the findings presented, here, will most likely lead to advances for various photobioelectrodes or bioelectrodes based on DET.

Data availability

Data supporting this study are provided in the ESI† or upon reasonable request from the corresponding authors.

Author contributions

Sascha Morlock: conceptualization, validation, formal analysis, investigation, writing – original draft, writing – review & editing, and visualization. Senthil K. Subramanian: resources and writing – review & editing. Athina Zouni: writing – review & editing, supervision, and funding acquisition. Fred Lisdat: conceptualization, validation, writing – review & editing, supervision, and funding acquisition. The manuscript was written with the contributions of all authors. In addition, all authors have approved the final version of the manuscript.

Conflicts of interest

There are no conflicts to declare.

Acknowledgements

Technical support by Gesine Bartels and Julia Gaetcke is highly acknowledged. All authors welcome the Federal Ministry for Education and Research's financial support within project 031B0557A+B (Biotechnology 2020). Funding was also provided by the Deutsche Forschungsgemeinschaft under Germany's Excellence Strategy—Grant Nos. EXC 2008/1–390540038 (Gesine Bartels) and Sfb1078 (Humboldt Universität of Berlin), TP A5 (Julia Gaetcke). S. M. thanks the Institute for Biology of the Humboldt University of Berlin for awarding a scholarship.

References

1 A. H. Teodor and B. D. Bruce, *Trends Biotechnol.*, 2020, **38**, 1329.
2 W. Lubitz, M. Chrysina and N. Cox, *Photosynth. Res.*, 2019, **142**, 105.
3 N. J. Planavsky, D. Asael, A. Hofmann, C. T. Reinhard, S. V. Lalonde, A. Knudsen, X. Wang, F. Ossa Ossa, E. Pecoits, A. J. B. Smith, N. J. Beukes, A. Bekker, T. M. Johnson, K. O. Konhauser, T. W. Lyons and O. J. Rouxel, *Nat. Geosci.*, 2014, **7**, 283.
4 V. M. Friebe and R. N. Frese, *Curr. Opin. Electrochem.*, 2017, **5**, 126.
5 K. Nguyen and B. D. Bruce, *Biochim. Biophys. Acta*, 2014, **1837**, 1553.
6 J. Barber, *Chem. Soc. Rev.*, 2009, **38**, 185.
7 M. T. Robinson, E. A. Gizzie, F. Mwambutsa, D. E. Cliffel and G. K. Jennings, *Curr. Opin. Electrochem.*, 2017, **5**, 211.
8 E. Musazade, R. Voloshin, N. Brady, J. Mondal, S. Atashova, S. K. Zharmukhamedov, I. Huseynova, S. Ramakrishna, M. M. Najafpour, J.-R. Shen, B. D. Bruce and S. I. Allakhverdiev, *J. Photochem. Photobiol., C*, 2018, **35**, 134.
9 J. Z. Zhang and E. Reisner, *Nat. Rev. Chem.*, 2020, **4**, 6.
10 R. E. Blankenship, D. M. Tiede, J. Barber, G. W. Brudvig, G. Fleming, M. Ghirardi, M. R. Gunner, W. Junge, D. M. Kramer, A. Melis, T. A. Moore, C. C. Moser, D. G. Nocera, A. J. Nozik, D. R. Ort, W. W. Parson, R. C. Prince and R. T. Sayre, *Science*, 2011, **332**, 805.
11 N. Torabi, S. Rousseva, Q. Chen, A. Ashrafi, A. Kermanpur and R. C. Chiechi, *RSC Adv.*, 2022, **12**, 8783.
12 D. Ciornii, S. C. Feifel, M. Hejazi, A. Kölsch, H. Lokstein, A. Zouni and F. Lisdat, *Phys. Status Solidi A*, 2017, **214**, 1700017.
13 K. D. Wolfe, A. Gargye, F. Mwambutsa, L. Than, D. E. Cliffel and G. K. Jennings, *Langmuir*, 2021, **37**, 10481.
14 H. Barhom, C. Carmeli and I. Carmeli, *J. Phys. Chem. B*, 2021, **125**, 722.
15 D. Ciornii, M. Riedel, K. R. Stieger, S. C. Feifel, M. Hejazi, H. Lokstein, A. Zouni and F. Lisdat, *J. Am. Chem. Soc.*, 2017, **139**, 16478.
16 M. Riedel, J. Wersig, A. Ruff, W. Schuhmann, A. Zouni and F. Lisdat, *Angew. Chem., Int. Ed.*, 2019, **58**, 801.
17 V. Hartmann, D. Harris, T. Bobrowski, A. Ruff, A. Frank, T. Günther Pomorski, M. Rögner, W. Schuhmann, N. Adir and M. M. Nowaczyk, *J. Mater. Chem. A*, 2020, **8**, 14463.
18 W. Tian, H. Zhang, J. Sibbons, H. Sun, H. Wang and S. Wang, *Adv. Energy Mater.*, 2021, **11**, 2100911.
19 R. A. Voloshin, S. M. Shumilova, E. V. Zadneprovskayaa, S. K. Zharmukhamedov, S. Alwasel, H. Hou and S. I. Allakhverdiev, *Photosynt.*, 2022, **60**, 121.
20 K. P. Sokol, W. E. Robinson, J. Warnan, N. Kornienko, M. M. Nowaczyk, A. Ruff, J. Z. Zhang and E. Reisner, *Nat. Energy*, 2018, **3**, 944.
21 X. Fang, K. P. Sokol, N. Heidary, T. A. Kandiel, J. Z. Zhang and E. Reisner, *Nano Lett.*, 2019, **19**, 1844.
22 V. M. Friebe, J. D. Delgado, D. J. K. Swainsbury, J. M. Gruber, A. Chanaewa, R. van Grondelle, E. von Hauff, D. Millo, M. R. Jones and R. N. Frese, *Adv. Funct. Mater.*, 2016, **26**, 285.
23 R. Białek, V. Friebe, A. Ruff, M. R. Jones, R. Frese and K. Gibasiewicz, *Electrochim. Acta*, 2020, **330**, 135190.
24 D. Jun, S. Zhang, A. J. Grzędowski, A. Mahey, J. T. Beatty and D. Bizzotto, *iScience*, 2021, **24**, 102500.
25 A.-M. Carey, H. Zhang, D. Mieritz, A. Volosin, A. T. Gardiner, R. J. Cogdell, H. Yan, D.-K. Seo, S. Lin and N. W. Woodbury, *ACS Appl. Mater. Interfaces*, 2016, **8**, 25104.
26 D. Pankratov, G. Pankratova and L. Gorton, *Curr. Opin. Electrochem.*, 2020, **19**, 49.
27 N. S. Weliwatte, M. Grattieri and S. D. Minteer, *Photochem. Photobiol. Sci.*, 2021, **20**, 1333.
28 J. Lee, H. Shin, C. Kang and S. Kim, *ChemSusChem*, 2021, **14**, 2216.
29 M. J. Kim, S. Lee, C.-K. Moon, J.-J. Kim, J. R. Youn and Y. S. Song, *Nano Lett.*, 2020, **20**, 4286.
30 Y. Shlosberg, B. Eichenbaum, T. N. Tóth, G. Levin, V. Liveanu, G. Schuster and N. Adir, *iScience*, 2021, **24**, 101892.
31 P. Bombelli, T. Müller, T. W. Herling, C. J. Howe and T. P. J. Knowles, *Adv. Energy Mater.*, 2015, **5**, 1.
32 K. Hasan, V. Grippo, E. Sperling, M. A. Packer, D. Leech and L. Gorton, *ChemElectroChem*, 2017, **4**, 412.
33 K. R. Stieger, D. Ciornii, A. Kölsch, M. Hejazi, H. Lokstein, S. C. Feifel, A. Zouni and F. Lisdat, *Nanoscale*, 2016, **8**, 10695.
34 P. Wang, F. Zhao, A. Frank, S. Zerria, A. Lielpetere, A. Ruff, M. M. Nowaczyk, W. Schuhmann and F. Conzuelo, *Adv. Energy Mater.*, 2021, **11**, 2102858.
35 A. Singh, S. Mandal, S. Chen, M. Liu, C. J. Gisriel, A.-M. Carey, H. Yan, D.-K. Seo, S. Lin and N. W. Woodbury, *ACS Appl. Electron. Mater.*, 2021, **3**, 2087.
36 Y. Yoneda, A. Goto, N. Takeda, H. Harada, M. Kondo, H. Miyasaka, Y. Nagasawa and T. Dewa, *J. Phys. Chem. C*, 2020, **124**, 8605.
37 K. R. Stieger, S. C. Feifel, H. Lokstein, M. Hejazi, A. Zouni and F. Lisdat, *J. Mater. Chem. A*, 2016, **4**, 17009.
38 D. Ciornii, A. Kölsch, A. Zouni and F. Lisdat, *Nanoscale*, 2019, **11**, 15862.
39 Y. Takekuma, H. Nagakawa, T. Noji, K. Kawakami, R. Furukawa, M. Nango, N. Kamiya and M. Nagata, *ACS Appl. Energy Mater.*, 2019, **2**, 3986.
40 Y. Takekuma, N. Ikeda, K. Kawakami, N. Kamiya, M. Nango and M. Nagata, *RSC Adv.*, 2020, **10**, 15734.
41 S. Morlock, S. K. Subramanian, A. Zouni and F. Lisdat, *ACS Appl. Mater. Interfaces*, 2021, **13**, 11237.

42 D. Ciornii, A. Kölsch, A. Zouni and F. Lisdat, *Electrochim. Acta*, 2019, **299**, 531.
43 K. R. Stieger, S. C. Feifel, H. Lokstein and F. Lisdat, *Phys. Chem. Chem. Phys.*, 2014, **16**, 15667.
44 D. Mersch, C.-Y. Lee, J. Z. Zhang, K. Brinkert, J. C. Fontecilla-Camps, A. W. Rutherford and E. Reisner, *J. Am. Chem. Soc.*, 2015, **137**, 8541.
45 S. C. Feifel, K. R. Stieger, M. Hejazi, X. Wang, M. Ilbert, A. Zouni, E. Lojou and F. Lisdat, *Electrochem. Commun.*, 2018, **91**, 49.
46 S. W. Hogewoning, E. Wientjes, P. Douwstra, G. Trouwborst, W. van Ieperen, R. Croce and J. Harbinson, *Plant Cell*, 2012, **24**, 1921.
47 A. H. Teodor, B. D. Sherman, Z. Y. Ison, E.-J. Ooi, J. J. Bergkamp and B. D. Bruce, *Catalysts*, 2020, **10**, 1016.
48 I. Domonkos, M. Kis, Z. Gombos and B. Ughy, *Prog. Lipid Res.*, 2013, **52**, 539.
49 R. J. Cogdell, *Philos. Trans. R. Soc., B*, 1978, **284**, 569.
50 A. Vershinin, *BioFactors*, 1999, **10**, 99.
51 (*a*) C. W. Mullineaux, *Photosynth. Res.*, 2008, **95**, 175; (*b*) A. N. Glazer, *Annu. Rev. Biophys. Biophys. Chem.*, 1985, **14**, 47.
52 K. Gundlach, M. Werwie, S. Wiegand and H. Paulsen, *Biochim. Biophys. Acta*, 2009, **1787**, 1499.
53 G. Amoruso, J. Liu, D. W. Polak, K. Tiwari, M. R. Jones and T. A. A. Oliver, *J. Phys. Chem. Lett.*, 2021, **12**, 5448.
54 H. Nagakawa, A. Takeuchi, Y. Takekuma, T. Noji, K. Kawakami, N. Kamiya, M. Nango, R. Furukawa and M. Nagata, *Photochem. Photobiol. Sci.*, 2019, **18**, 309.
55 P. K. Dutta, S. Lin, A. Loskutov, S. Levenberg, D. Jun, R. Saer, J. T. Beatty, Y. Liu, H. Yan and N. W. Woodbury, *J. Am. Chem. Soc.*, 2014, **136**, 4599.
56 P. I. Gordiichuk, D. Rimmerman, A. Paul, D. A. Gautier, A. Gruszka, M. Saller, J. W. de Vries, G.-J. A. H. Wetzelaer, M. Manca, W. Gomulya, M. Matmor, E. Gloukhikh, M. Loznik, N. Ashkenasy, P. W. M. Blom, M. Rögner, M. A. Loi, S. Richter and A. Herrmann, *Bioconjugate Chem.*, 2016, **27**, 36.
57 G. Kasagi, Y. Yoneda, M. Kondo, H. Miyasaka, Y. Nagasawa and T. Dewa, *J. Photochem. Photobiol., A*, 2021, **405**, 112790.
58 S. Morlock, S. K. Subramanian, A. Zouni and F. Lisdat, *Biosens. Bioelectron.*, 2022, **214**, 114495.
59 J. Kern, B. Loll, C. Lüneberg, D. DiFiore, J. Biesiadka, K.-D. Irrgang and A. Zouni, *Biochim. Biophys. Acta*, 2005, **1706**, 147.
60 A. Kölsch, M. Hejazi, K. R. Stieger, S. C. Feifel, J. F. Kern, F. Müh, F. Lisdat, H. Lokstein and A. Zouni, *J. Biol. Chem.*, 2018, **293**, 9090.
61 F. Müh and A. Zouni, *Biochim. Biophys. Acta*, 2005, **1708**, 219.
62 T. Bennett, H. Niroomand, R. Pamu, I. Ivanov, D. Mukherjee and B. Khomami, *Phys. Chem. Chem. Phys.*, 2016, **18**, 8512.
63 F. Zhao, A. Ruff, M. Rögner, W. Schuhmann and F. Conzuelo, *J. Am. Chem. Soc.*, 2019, **141**, 5102.
64 K. P. Sokol, D. Mersch, V. Hartmann, J. Z. Zhang, M. M. Nowaczyk, M. Rögner, A. Ruff, W. Schuhmann, N. Plumeré and E. Reisner, *Energy Environ. Sci.*, 2016, **9**, 3698.